Semiconductor-Based Photocatalytic Oxygen Evolution Performance for Water Splitting: Light-Driven Energy Conversion and Storage

Habib Gemechu, Kebede Bekele, Woldesenbet Bafe, Prawesti Ambar, Rapita Astriani, Farghani Fariz, Farah Meutia, and Riski Titian Ginting

Abstract Global energy demand continues to rise due to population expansion and economic success. As a result, annual population increases require high energy demand to provide essential needs and perform daily processes. To achieve sustainable development, energy sources ought to be reliable and have slight environmental problem. Photocatalytic water splitting by producing H_2 is an alternative approach to replace the traditional fossil fuels and providing environment friendly energy storage. Design in photocatalysts is essential to achieve economically applicable photocatalytic water splitting with higher efficiency. Sustainable hydrogen production would be a crucial first step toward powering fuel-cells. In addition, implementation on a larger industrial scale for attaining mature technological operations to lower N_2 and CO_2 emissions while producing desired products is achieved. The main challenge is harnessing solar radiation to produce hydrogen from water. In the coming decades, it is anticipated that wind-powered electrolysis and photovoltaics will be prioritized for producing renewable hydrogen. However, integrating catalysis with light harvesting for photoelectrolysis has various benefits. Among those benefits, thermal management and employment of lower current densities are preferable. Nowadays, semiconductor photocatalysis using solar energy is considered as a prospective way for disbanding the environment pollution and the global energy crises. It has been thoroughly studied in a variety of photocatalysis domains, including the reduction of pollution, the production of H_2 and O_2, etc. The recent rising attention toward photocatalytic water splitting can be attributed to four-electron reaction mechanism.

Keywords OER · Water splitting · Photocatalysis · Energy · Storage

H. Gemechu · K. Bekele · W. Bafe · P. Ambar · R. Astriani · F. Fariz · F. Meutia
Department of Materials Science and Engineering, National Taiwan University of Science and Technology, Taipei 10672, Taiwan, ROC

R. T. Ginting (✉)
Department of Electrical Engineering, Universitas Prima Indonesia, Medan, Indonesia
e-mail: titiangt@unprimdn.ac.id

H. Abdullah (ed.), *Photocatalytic Activities for Environmental Remediation and Energy Conversion*, Green Energy and Technology,
https://doi.org/10.1007/978-981-19-6748-1_5

1 Introduction

Energy is required worldwide to provide basic needs like domestic activities and support high energy for industrial demands. The quality of energy in the development process is a critical matter. For sustainable development, energy sources are required to be safe and have less negative impact on the environment. Economic and social growth on the long term depends on the reliability and affordable access to the energy resources [1]. Global energy demand is still increasing as a result of population increase and economic success. The increasing energy crisis and environmental pollution due to excessive utilization of fossil fuels is detrimental to climate changes. Dependency on fossil fuels is urgently sought to be minimized by conducting research on an extended scale to explore alternative renewable and clean alternative energy resources. In addition to the renewable energy source, solar energy is widely abundant for tackling environmental concerns, because it is free and environmentally friendly. Solar fuel production from sunlight captured by man-made photocatalysts is both practical and highly desirable [2].

Researchers have studied solar energy conversion and storage techniques in depth in order to make the most of the massive quantity of energy of 4.3×10^{20} J h^{-1} that hits the surface of the Earth. Solar energy can be utilized for chemical conversion for energy storage or converted into electricity. Photocatalytic water splitting is a potential and environmentally friendly method of storing solar energy in the form of H_2. When used in fuel cells to produce electricity, H_2 is a green source of energy because the resultant byproduct is water. Additionally, hydrogen has a high energy density, ease of storage and transport with current technologies. Photocatalytic water splitting is conducted in an aqueous solution containing a photocatalyst to capture photonic energy and induces the water splitting process. Researchers have investigated and reported various materials that are capable of overcoming the thermodynamic and kinetic obstacles needed for photoconversion of solar energy via water splitting. Suitable energy band gap with appropriate CB and VB values, high resistivity of photocorrosion, and an adequate charge transfer system are all criterions for an effective photocatalyst [3].

Solar energy can be converted and stored into various beneficial forms of energy. It can be used in chemical fuel conversion via H_2 through solar water splitting, CH_4 production via solar-driven CO_2 reduction, and ammonia synthesis from N_2. Besides, it also generates electricity (photovoltaic effect) and heat production (thermal collectors or phase changing materials). H_2 fuel is an excellent approach as a green chemical energy carrier due to its high specific energy with byproducts containing only heat and water. The most promising method for generating H_2 is photocatalytic water splitting via solar energy. However, production of highly effective photocatalysts still faces significant technical challenges. Solar light-driven photocatalysts stand out as a solution to the recent energy and environment crisis. TiO_2 photoelectrode was first found to be capable of decomposing H_2O into H_2 and O_2 under UV irradiation in 1972. Since then photocatalytic semiconductors have gained extensive attention

toward environmental purging and energy conversion [4]. The photocatalytic process consists typically of 3 steps:

(i) Electron–hole pairs formation in the photocatalyst in response to light irradiation ($h\nu = E_g$);
(ii) The migration of the photogenerated species from the bulk to the surface of the photocatalyst; during this step some of the generated species are recombined; and
(iii) Non-recombination electrons and holes will interact with adsorbed reactants by either reduction or oxidation processes. Overall, photocatalytic water splitting ($H = 285.5$ kJ mol^{-1}) is thermodynamically hindered. Hydrogen evolution reaction (HER) and oxygen evolution reaction (OER), both two half reactions, sum up the Gibbs free energy via photon energy. Photocatalysts are irradiated with light-induced reduction and oxidation reactions in which the equations are as follows:

$$1.\ 2H^+ + 2e^- \rightarrow H_2 \quad \text{(reduction reaction)} \tag{1}$$

$$2.\ 4OH^- + 4h^+ \rightarrow O_2 + 2H_2O \quad \text{(oxidation reaction)} \tag{2}$$

OER in which $4e^-$ are transferred in the water splitting process is the rate determining step with a higher reaction barrier than HER. Bandgap values of the photocatalysts should be higher than 1.6 eV for enabling multi proton/electron processes of water oxidation. The bandgap value is essential to overcome the sluggish kinetics, which is referred to as the multistep reaction of the existing intermediates during the O_2 production process. The pH of the medium has an influence on the OER, and the equations are as follows:

$$2H_2O \rightarrow O_2 + 4e^- + 4H^+ \quad \text{(acidic condition)} \tag{3}$$

$$4OH^- \rightarrow O2 + 4e^- + 2H_2O^+ \quad \text{(alkaline condition)} \tag{4}$$

OER efficiency is influenced by various parameters such as illumination absorption, photogenerated charge separation, and the catalytic surface reaction, which are the three fundamentals of a photocatalytic process.

1.1 Water Splitting for Energy Conversion and Storage

Fossil fuels have been indiscriminately used to convert the chemical energy contained in these fuels into heat and power, thus dominating the global energy landscape, despite rapid depletion and the impact of carbon dioxide emissions on the Earth's climate. Since the 1970s, interest in renewable energy sources like wind, solar, and

biomass has increased, leading to the implementation of several strategies, many of which are ideal carbon neutral, meaning that only few CO_2 is released into the environment [5]. Limitations in energy storage technology and the degree of integration with the power grid system prevent these intermittent energy sources from being used to its full potential. An appealing approach to ensure a continuous, robust energy supply is the conversion of surplus electrical energy to chemical bonds (hydrogen gas, methane, and liquid ethanol) via electrochemical or photo-electrochemical conversion by renewable electricity or direct sunlight through water splitting as shown in Fig. 2. In this scenario, much of research interests focus on the well-known water splitting reaction [6]. This reaction can be described as two half-cell reactions as shown in Fig. 1; the oxygen evolution reaction (OER), as follows:

$$2H_2O \rightarrow 4H^+ + 4e + O_2 E^\circ = 1.23\,\text{V vs. NHE} \tag{5}$$

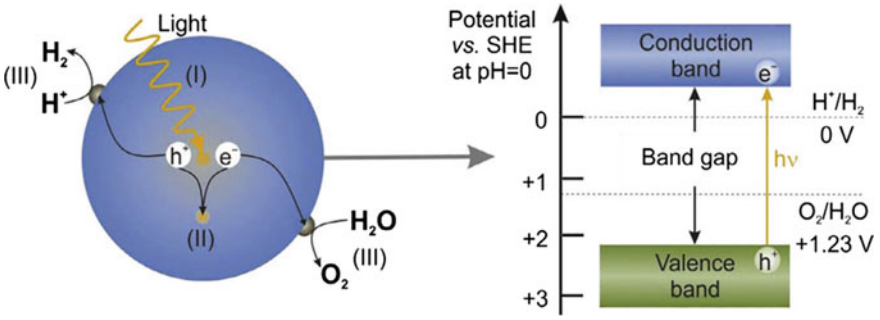

Fig. 1 The main processes and the principle of photocatalytic water splitting in semiconductor photocatalysts [2]

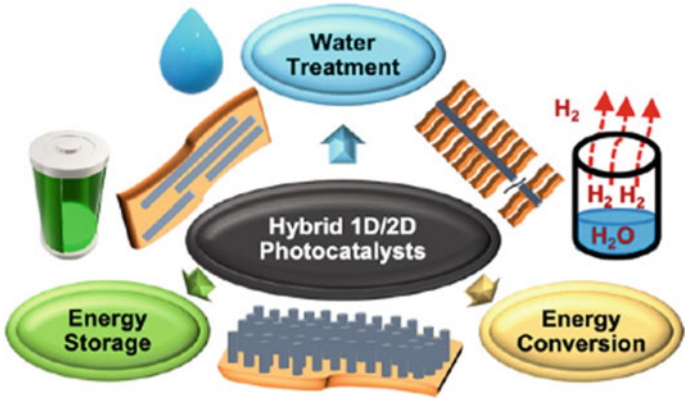

Fig. 2 Hybrid Photocatalyst for light harvesting water splitting for energy conversion and storage application

As well as the hydrogen evolution reaction:

$$\text{HER}, 2H^+ + 2e \rightarrow H_2E^\circ = 0.00\,\text{V vs. NHE} \tag{6}$$

$$\text{Overall}: \quad 2H_2O \rightarrow 2H_2 + O_2 \quad E^\circ\text{cell} = -1.23\,\text{V}; \; \text{DG} = 475\,\text{kJ/mol}$$

In either case, a suitable catalyst is required to lower the huge overpotential barrier, hence speeding up the electrochemical kinetics. A four proton-coupled electron transfer process and the formation of oxygen–oxygen bonds, both of which are necessary for the reaction, are required for the catalysis of OER, which is more complex and kinetically challenging, in contrast to the HER, which produces fuel relatively simple to implement. Typically, electrocatalysts (IrO_2, RuO_2, Ni oxides, etc.) are used in conventional electrochemical cells for water splitting to reduce overpotential and Tafel slope and maximize energy conversion efficiency. However, the onset potential at an electrocatalyst is always higher with respect to the theoretical redox potential of water oxidation (1.23 V vs. RHE) due to the thermodynamic energy barriers of this electrochemical reaction [7].

Photoreduction of excessive CO_2 emissions with greenhouse effects into combustible CO and CH_4. However, due to the strong linear structure of CO_2, obtaining a highly efficient CO_2 reduction under visible-light irradiation is difficult. Furthermore, an effective CO_2 reduction photocatalyst should have appropriate redox potentials, high charge separation efficiency, and a long lifetime. The range of light absorption can be expanded using 1D/2D heterostructured photocatalysts, which can also affecting separation and migration of photoinduced charge carriers [4]. For instance, through a spatial distribution heterojunction made possible by the in situ growth of $ZnIn_2S_4$ (ZIS) nanosheets on g-C_3N_4 micro tubes (TCN), highly efficient charge separation, rapid interfacial charge transfer, strong light absorption, and larger CO_2 adsorption are required for photocatalytic CO_2 reduction. The vertically aligned $ZnIn_2S_4$ nanosheets on both the outer and inner surfaces of TCN generate a hierarchical core/shell structure, which increases the conversion efficiency of CO_2 to 1453 and 863 μmol g^{-1} h^{-1} of CO and H_2, respectively, which are 4.3 and 5 times higher than those of a bulk CN/ZIS heterojunction. Many reports such as the conversion of CO_2 to CH_4 or CO and H_2 production are available in these contexts. For instance, it is critical to collect solar energy during the day and then use it with a high conversion efficiency at night. Because phase-change materials have high phase-change enthalpies, acceptable phase-change temperatures, and modest volume expansion/shrinkage, they are frequently employed for solar-thermal energy storage [8].

1.2 Fundamental Processes and Mechanism in Photocatalytic Overall Water Splitting

Water splitting is a thermodynamically unfavorable reaction that needs more energy than 1.23 eV to proceed. Because every oxygen molecule needs four holes, water oxidation is more difficult than H_2 reduction in an artificial manner and five times slower than the hydrogen evolution process. There are several crucial phases involved in photocatalytic water splitting. Understanding the mechanism of each phase and identifying the important parameters impacting the process efficacy are critical when creating photocatalysts for this process. H_2 is a carbon-free, clean fuel with a high specific enthalpy [9]. Previously, roughly 95% of the world's hydrogen fuel was mostly generated from natural gas, but now, by combining methane with the steam utilizing fossil fuel, hydrogen and carbon dioxide CO_2 may be produced. As a result, hydrogen generation from methane is a fossil fuel product rather than a sustainable energy source. The key to utilizing hydrogen generation is to develop an efficient H_2-preparation technology that does not require the use of fossil fuels. The method using photocatalytic materials to produce hydrogen has been demonstrated since 1972 according to the following reaction equation,

$$2H_2O \rightarrow 2H_2 + O_2 \tag{7}$$

$$\Delta E^{\circ} = 1.23\,\text{ev},\ \Delta G^{\circ} = +237.2\,\text{kJ/mol}$$

This photocatalytic process is driven by a thermodynamic "uphill reaction" of solar energy with a large change of $\Delta G^0 = 1.23$ eV (237.13 kJ mol^{-1}) per photon.

There are three major steps to an overall photocatalytic split water for a semiconductor photocatalyst:

(1) the absorption of photons with the right energy on a semiconductor's surface, which can promote electron transfer from the valence band position to the conduction band position and generate electron–hole pairs (e^-/h^+);
(2) The separation and migration of charge carriers in a brief period of time on the material's surface; and
(3) The impingement between the corresponding free electrons and holes on the system surface to complete the water splitting reaction. On the other hand, the recombination of the free electrons and the excited holes may readily happen in the second step, giving rise to a poor photocatalytic activity of the nanocrystal surface. Therefore, even at a low solar energy flux density, the appropriate bandgap and the matching levels of the conduction and valence bands might facilitate light absorption on the surface of the semiconductor photocatalyst. In order to drive the electrons to the empty CB position from the filled valence band position of the semiconductor photocatalyst, the absorbed photon must have a higher energy than the corresponding bandgap of the semiconductor [10].

Subsequently, the excited electrons and holes pair (e^-/h^+) is formed according to the following expression,

$$\text{Photon activation: Semiconductor} + h\nu \rightarrow e^- + h^+,$$
$$\text{Oxygen adsorption}: (O_2)_{ads} + e^- \rightarrow O_2^{\cdot -},$$
$$\text{Water ionization}: H_2O \rightarrow OH^- + H^+,$$
$$\text{Superoxide protonation}: O_2^{\cdot -} + H^+ \rightarrow HOO^{\cdot}.$$

The bandgap energy should be more than 1.23 V from a thermodynamic perspective, and the band positions should be below 1.23 V versus normal hydrogen electrode (NHE) to share electrons from water O^{2-} anions and above 0.0 V versus NHE to decrease water H^+ ions. After light has been absorbed, electrons are moved to the conduction band and holes are simultaneously formed at the valence band. In order to carry the redox processes, photogenerated charge carriers must recombine in the bulk or on the surface. In the presence of metal particles with a larger work function than the oxide semiconductor, excited electrons may be pumped in order to speed up charge separation and convert H^+ ions into atomic hydrogen, which will subsequently mix with other molecules to form H^{2+}. At the energy level of the valence band, electrons are abstracted from O_2- anions of water to close the cycle. Accordingly, the reaction products desorb from the catalyst surface and are transferred to the medium to complete the overall process [11].

The fundamental concept of photocatalytic water splitting in semiconductor photocatalysis is depicted in Fig. 3. Absorption of photons creates pairs of electrons and holes in the first step (I) which will be recombine or separate and move to the reaction sites (II). Finally, water molecules react with electrons or holes to produce H_2 or O_2 (III). The highest occupied molecular orbital (HOMO, top of the valence band in a periodic crystal perspective) is excited to the lowest unoccupied molecular orbital (LUMO, bottom of the conduction band), leading to the generation of excitons, or excited electron–hole pairs. This step indicated that incident photon gives enough energy above the optical gap (also known as the absorption onset) of the irradiated photocatalyst. The excess energy known as the exciton binding energy, is converted into free electrons and holes (where "free" refers to non-bonded excitons). The band gap is defined as the optical band plus the exciton binding energy. At the same time, the potential of the CB should be more negative than the reduction potential of H_2O/H_2 (0 V vs. NHE, pH = 0), while the VB should be more positive than the oxidation potential of O_2/H_2O (1.23 V vs. NHE, pH = 0). Therefore, the theoretical minimum band gap for water splitting is 1.23 eV. The width of the band gap and the levels of the CB and VB are extremely important for semiconductor photocatalysts, which are essential for the second and the third step. These free charge carriers can drive redox reaction in photocatalytic water splitting, but also reform excitons in a process commonly referred to as electron–hole recombination [2] (Scheme 1).

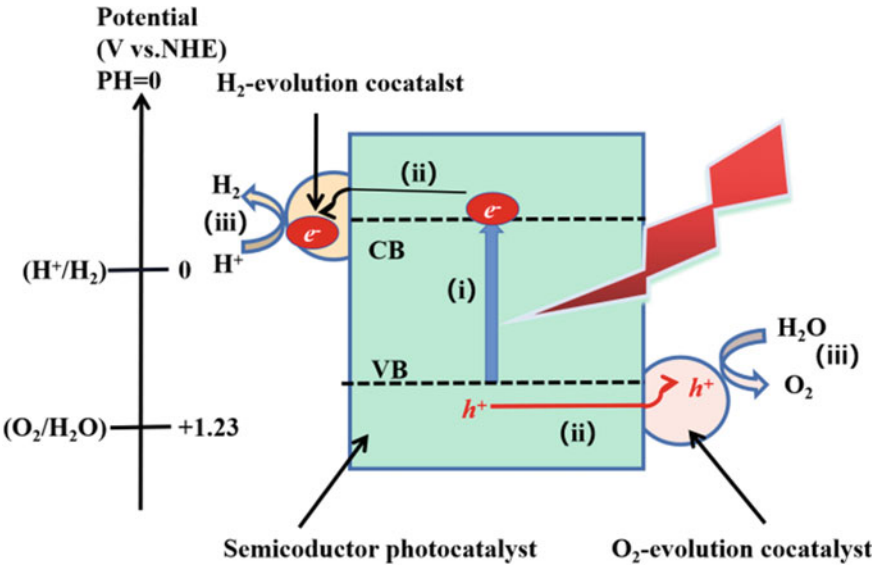

Fig. 3 Schematic diagram of the three major steps of the overall photocatalytic water splitting on a semiconductor photocatalyst

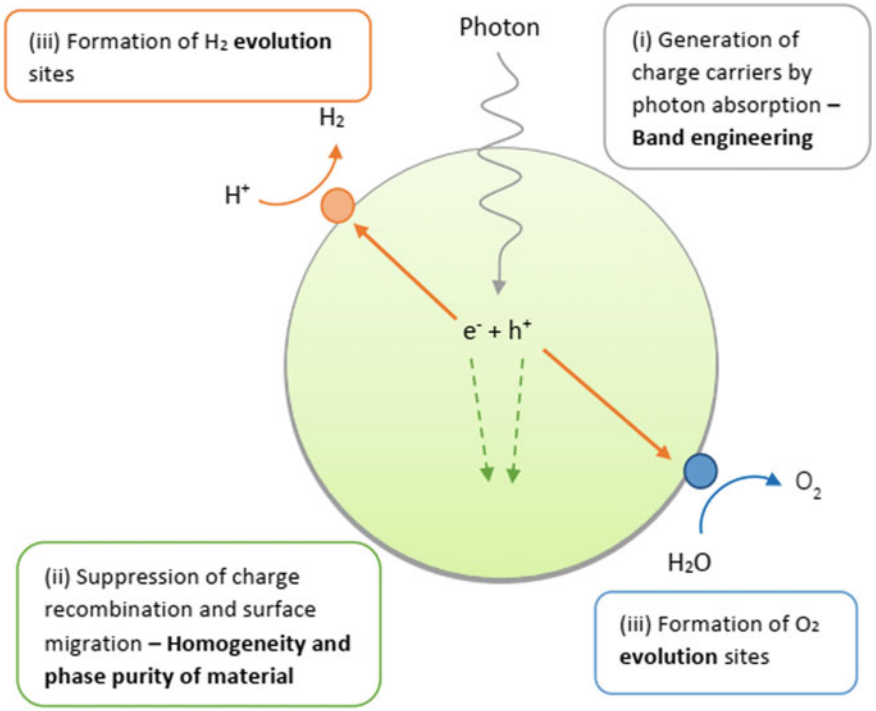

Scheme 1 Schematic illustration of three primary steps of photocatalytic water splitting [12]

1.3 Fundamental of Photocatalysis Based on Semiconductors

In general, the photocatalyst is activated by visible light, which leads to the generation of electron–hole pairs that are formed by the migration of generated electrons from the valence band (VB) to the conduction band (CB) of a semiconductor photocatalyst [13]. In a crystal, the valence band VB, the highest occupied band, the conduction band CB, and the lowest empty band are separated by a band gap in the so called region of forbidden energies. The bandgap model describes a photocatalytic system based on a semiconductor in which these two bands are separated by a band gap, a region of forbidden energies [14]. An electron that is excited to the CB leaves a hole (h^+) in the VB when the incident energy is equal to or larger than the band gap of the semiconductor, as depicted in Fig. 4.

Lower level of CB that is located at a more negative potential than the electrochemical potential of the desired reaction is the photoexcited electron used in a reduction reaction with an electron acceptor. For instance, the reduction of protons to hydrogen, production of an O_2-ion radical, and CO_2 reduction. The photo-generated hole in the semiconductor VB can also engage in an oxidative reaction with an electron donor with oxidation potential that is more negative than the maximum VB. In systems designed for the production of green fuel and other environmental applications, the semiconductor properties is the most crucial part (Fig. 5).

A wide range of semiconductors are now being synthesized and investigated in order to increase their performance, while novel architectures are being prepared and developed at the same time. The photocurrent density generated by the photocatalyst device is the performance benchmark; it should be greater than 10 mA/cm^2 in order to be useful in an industrial application. However, the device stability over a long period of time and continuous operation are required. Semiconductors can be categorized as follows in this context: (i) single crystal versus nanostructured and (ii) narrow against wide band gap. Single crystals (Si, GaAs and GaP) feature a high diffusion length and high mobility, while nanostructured materials exploit the small distance necessary to achieve a highly efficient rate of charge transfer (e−/h^+). A large band

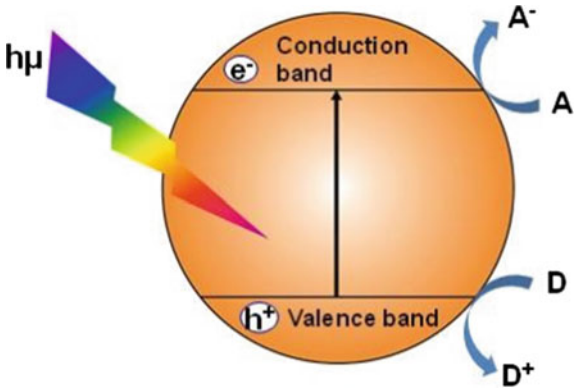

Fig. 4 Schematic illustion of electron–hole generation after adsorbed photon energy (hv) in an inorganic photosystem [14]

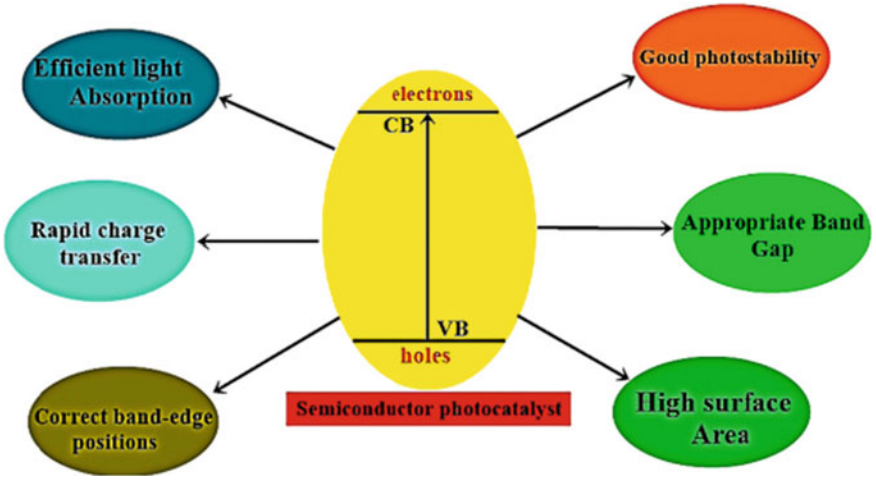

Fig. 5 The foremost properties of a noble photocatalyst

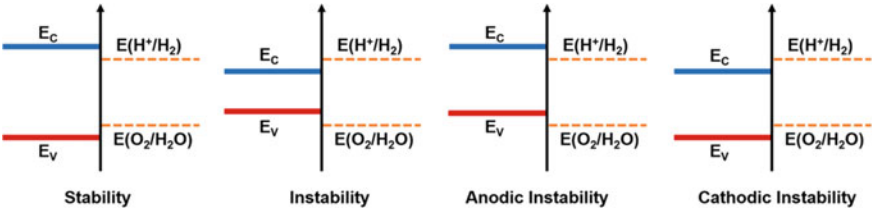

Fig. 6 Comparison in stability of semiconductor for the water splitting process's redox potential

gap (Eg) absorbs a narrow portion of the light spectrum, leading to poor absorption, whereas a tiny band gap absorbs a greater portion of the spectrum. Additionally, a wider band gap tends to resist photocorrosion, whereas a narrower band gap is more prone to it. The Ec and Ev bracket are the E(H/H_2) and the E(O2/H2O), respectively, which sums up the optimal conditions for semiconductor stability. Photocorrosion will occur due to several issues [15]. Figure 6 displays the stability of semiconductors in relation to the redox potential of water splitting.

1.4 Harvesting and Storing Solar Energy

The ultimate solution to the ever-increasing global energy need is to harvest electricity directly from photon energy utilizing photovoltaic (PV) systems. For improved usage of the copious but occasionally available sunlight, simultaneous solar energy conversion and storage is gaining a lot of attention. Photoelectrodes drive non-spontaneous reversible redox reactions in solar-powered redox cells (SPRCs), which can give

energy via the related reverse reactions. This is a cost-effective and promising method for direct solar energy collection and storage. However, the lack of photoelectrodes having both high conversion efficiency and high durability becomes a bottleneck that hindered practical applications of SPRCs [16].

Due to its potential to address the world energy crisis, energy harvesting technology with a clean and renewable energy source has attracted a lot of interest. Solar energy is the most attractive among the renewable energy sources as compared to wind, geothermal, hydropower, and many others, since it can provide sustainable power by using hydrogen gas as an energy carrier. Practically, substantial advancements have been made in the photoelectrochemical (PEC) water splitting method of producing hydrogen from water using solar energy. The photoelectrodes (photoanode or photocathode), electrolyte, and light source make up the majority of the PEC water splitting system. Generally, light-absorbing semiconductors have been used as the photoelectrode and the electrode materials are the main research topics in the field of PEC water splitting [17] (Fig. 7).

Solar and wind energy can be distributed locally via the off grid system, thus reducing the need for costly transmission lines while also improves energy security. At larger scales, it is possible to harvest solar energy for local usage. Utility scale PV can enable micro-grids that can deliver dispatchable electricity to nearby towns when combined with other energy sources (such as wind, chemical fuels, and hydropower) and energy storage devices. Due to the high cost of maintaining transmission lines, this strategy can be effective, especially for isolated communities. An alternative for families to install PV modules on their rooftops and use batteries to store energy for use later, in the event that solar generating is no longer feasible (i.e., load shifting of daytime generation to night-time).

However, the solar-powered gadgets or appliances that can be used by following procedures:

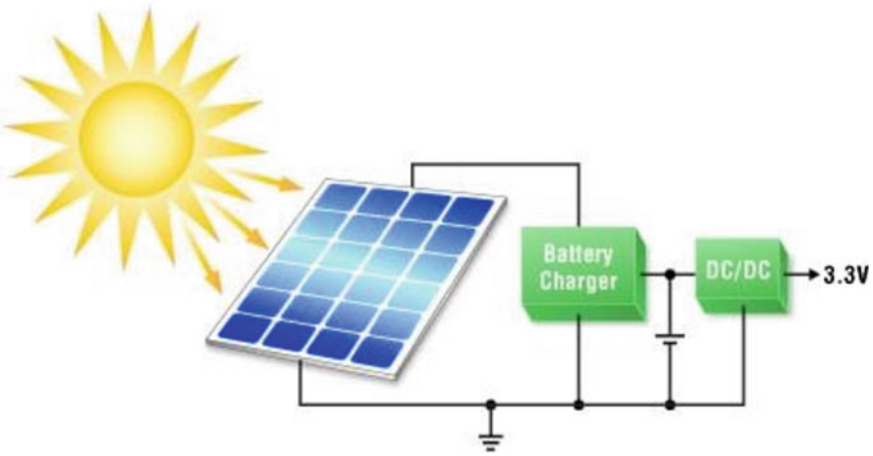

Fig. 7 Solar Harvesting energy system (*Source* Linear Technology)

(i) directly gather solar energy and.
(ii) electrochemically store that energy is another intriguing potential.
(iii) supply electricity to power a load.

New opportunities such as low power electronics applications, remotely powered sensors, electrochromic smart windows, remote antenna tracking devices, and self-charging wearable electronics may arise from the seamless integration of solar powered gadgets. The terms photorechargeable energy storage systems, hybrid solar energy conversion/harvesting and storage systems, and solar batteries have all been used to refer to these integrated solar energy conversion and storage systems. Since the early 1970s, there have been reports of hybrid systems that can power electronics while also collecting solar energy and storing it electrochemically [18].

2 Photocatalysts for Oxygen Evolution

Numerous photocatalysts (e.g., ZnO, CdS, WO_3, and $SrTiO_3$) have been intensively researched for water splitting applications since the pioneering work by Fujishima and Honda on water splitting to create H_2 and O_2 under UV irradiation based on TiO_2 photoelectrode. Despite extensive investigation, majority of the photocatalysts produced are not suitable for visible-light-induced water splitting due to inadequate light utilization or photostability. Furthermore, the high recombination rate of photoexcited electron–hole pairs generated by an unfavorable band structure severely limits their practical applications [4]. Alternatively, photocatalysts with a band gap of approx. 1.23 eV and no photocorrosion are suitable for overall water splitting. To reduce the recombination of photogenerated electrons and holes during water splitting, high crystallinity and smaller particle size are preferred.

As water splitting catalysts, metal oxides, sulfides, nitrides, and phosphates with d^0 and d^{10} metal cations have been used. Perovskite materials made of Group I and Group II metals, as well as some lanthanides, can be utilized to catalyze photochemical water splitting. Figure 8 summarizes the band structure of various types of semiconductors in relation to the redox potentials of water splitting. To improve solar energy efficiency, modification of photocatalysts by doping with some transition metal cations such as Ni^{2+}, Cr^{3+}, and V^{5+} can help to increase the visible light response. To inhibit the energy decreasing backward reaction of water splitting and increase the hydrogen production yield, suitable cocatalysts including RuO_2, NiO, Au, and Pt were widely used.

2.1 Tio_2-Based Photocatalysts

Since the first report by Fujishima and Honda in the late twentieth century, the TiO_2-based photocatalyst has emerged as a viable material for renewable fuel production

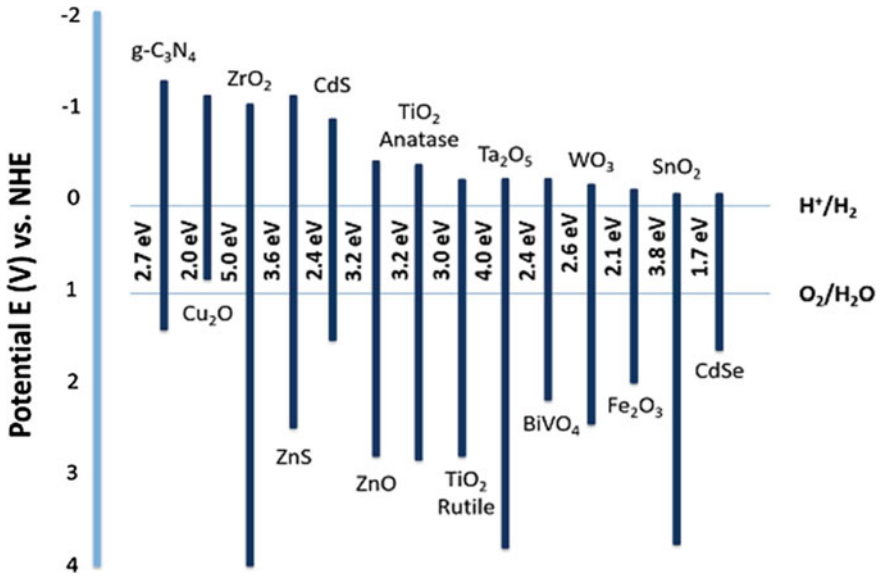

Fig. 8 Various band structures of semiconductors with the redox potentials for water splitting

and environmental remediation. As a result of its unique qualities (e.g., remarkable electrical properties, stability, eco-friendliness, and cost-effectiveness), TiO_2-based photocatalysts have been the most researched materials for photocatalytic applications in a recent study [13]. Improvements in three different pathways have been prioritized in the development of TiO_2-based photocatalysts: (i) the development of visible light-active TiO_2; (ii) the enhancement of photogenerated electron–hole separation using anatase–rutile homojunction; and (iii) the use of TiO_2-based nanocomposite. The gradient doping with nonmetallic heteroatoms in TiO_2 has been developed to improve the electronic structure with extensive efforts in elemental doping. When photons with energy (E = hv) equal to or greater than the band gap (3 eV for rutile and 3.2 eV for anatase phase) are absorbed by a semiconductor such as n-TiO_2, the photoactivity of the semiconductor is initiated, and a small percentage of electrons and holes are formed [19]. Small fraction of charge carriers can only reach the surface, which react with adsorbed molecules or ions, depending on the density of states (Fig. 9).

Despite its chemical stability in electrolyte solutions, n-TiO_2 has a number of drawbacks, and is able to only absorb 3% of solar irradiation. In order to improve the usability of n-TiO_2 as a water splitting catalyst, the improvement of its photosensitivity in the UV region and simultaneous shift in the spectral response to the visible region (400 nm–800 nm) have been performed. The best approach to meet this challenge is by doping n-TiO_2 with different elements (metal and nonmetals) and thus decrease its photo threshold energy. Transition metals have been used intensively as impurities dopands for n-TiO_2. Mixed results were reported for improving

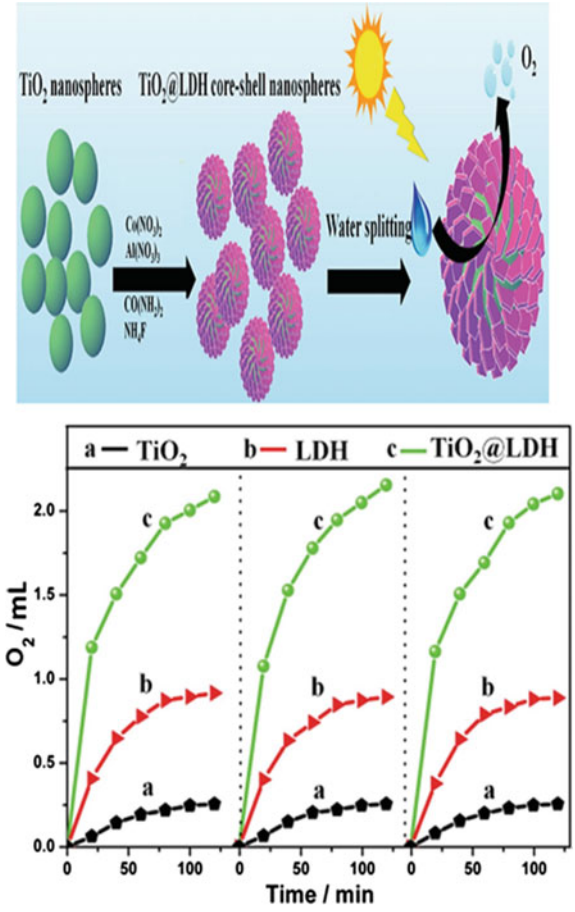

Fig. 9 **a** Schematic illustration of TiO_2@CoAl-LDH core–shell nanospheres toward O_2 from splitting of water (I), volume of O_2 generation as function of irradiation time ($\lambda > 200$ nm) in three consecutive cycles for a) TiO_2 nanospheres; **b** CoAl-LDH nanoplatelets; **c** TiO_2@LDH nanospheres, respectively (II)

the spectral response of metal doped Titania [20]. Dou et al. used a simple two-step method to make TiO@CoAl-LDH core–shell nanospheres: hydrothermal synthesis of TiO_2 hollow nanospheres followed by in situ growth of CoAl LDH shell (Fig. 9a). Under visible light illumination, the resultant material has an extraordinary high photocatalytic activity for oxygen evolution from water splitting, with O_2 generation rates of 2.34 and 2.24 mmol h^{-1} g^{-1}.

The broad spectrum absorption and strong electronic coupling between TiO_2 core and CoAl-LDH shell allow for improved solar energy and rapid electron–hole separation, resulting in significant photocatalytic activity toward oxygen generation. Furthermore, the TiO_2@CoAl-LDH photocatalyst produced has good recyclability and stability. TiO_2@CoAl-LDH nanospheres were prepared via two-step hydrothermal synthesis with TiO_2 hollow nanospheres as the core and in situ growth of CoAl-LDH as the shell. Figure 10 shows the XRD pattern of the resulting TiO_2@CoAl-LDH, with pristine TiO_2 and CoAl-LDH as reference samples. To better

understand the interaction between the CoAl-LDH shell and TiO_2 core in Fig. 11, a narrow-scan X-ray photoelectron spectroscopy (XPS) as shown in Fig. 12 was used. For the CoAl-LDH sample, the binding energies at 781.3 and 797.3 eV correspond to Co $2p_{3/2}$ and Co $2p_{1/2}$, respectively. The appearance of satellite and 803.3 eV implies the presence of a high-spin divalent state of Co^{2+} in this sample. For the TiO_2@LDH nanospheres, however, the binding energies of Co $2p_{3/2}$ and Co $2p_{1/2}$ shift to 781.7 and 797.6 eV, respectively (Fig. 12a).

The binding energies of Ti $2p_{3/2}$ and Ti $2p_{1/2}$ of TiO_2@LDH nanospheres demonstrate a negative shift compared with those of pristine TiO_2 microspheres (Fig. 12b). In addition, the increased and decreased binding energies of Co 2p and Ti 2p indicate an obvious electron transfer from the LDH shell to the TiO_2 core. The strong electronic coupling between LDH and TiO_2 would probably accelerate the electron–hole separation [21]. Water-splitting on TiO_2: mechanism, reduction, and oxidation are fundamental chemical processes involved in water splitting. Previously, in order to produce H_2 and O_2, the semiconductor positions CB and VB must both fall within the potential windows of water reduction and oxidation potential, respectively. When light strikes TiO_2, electrons in the VB travel to the CB and holes are created. Excited electrons promote the production of hydrogen, whereas holes aid in the production of oxygen (Fig. 13).

The valence band of TiO_2 is more positive than E^0oxid of O_2/H_2O (1.23 V vs. NHE, pH = 0), while the conduction band is more negative than E^0 red of H^+/H_2 (0 eV vs. NHE, pH = 0). However, there are two fundamental drawbacks to TiO_2 materials. Firstly, rapid charge carrier recombination cause undesired energy to be released. Secondly, the poor visible light harvesting ability such as TiO_2 can only be

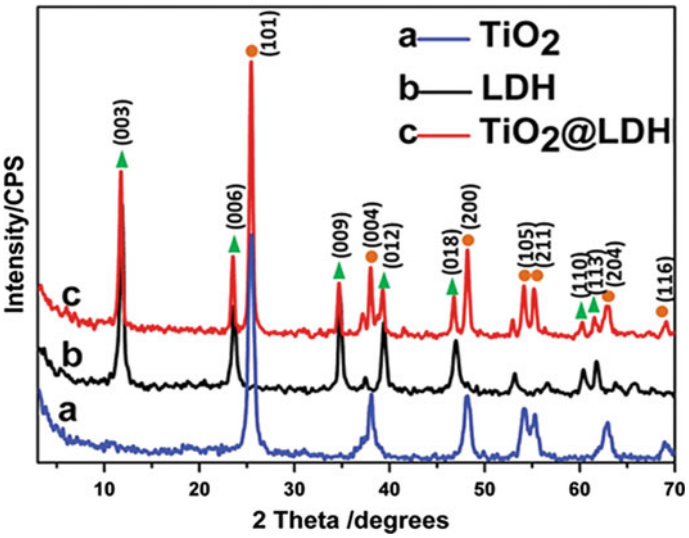

Fig. 10 XRD pattern of TiO_2@CoAl-LDH, with pristine TiO_2 and CoAl-LDH [21]

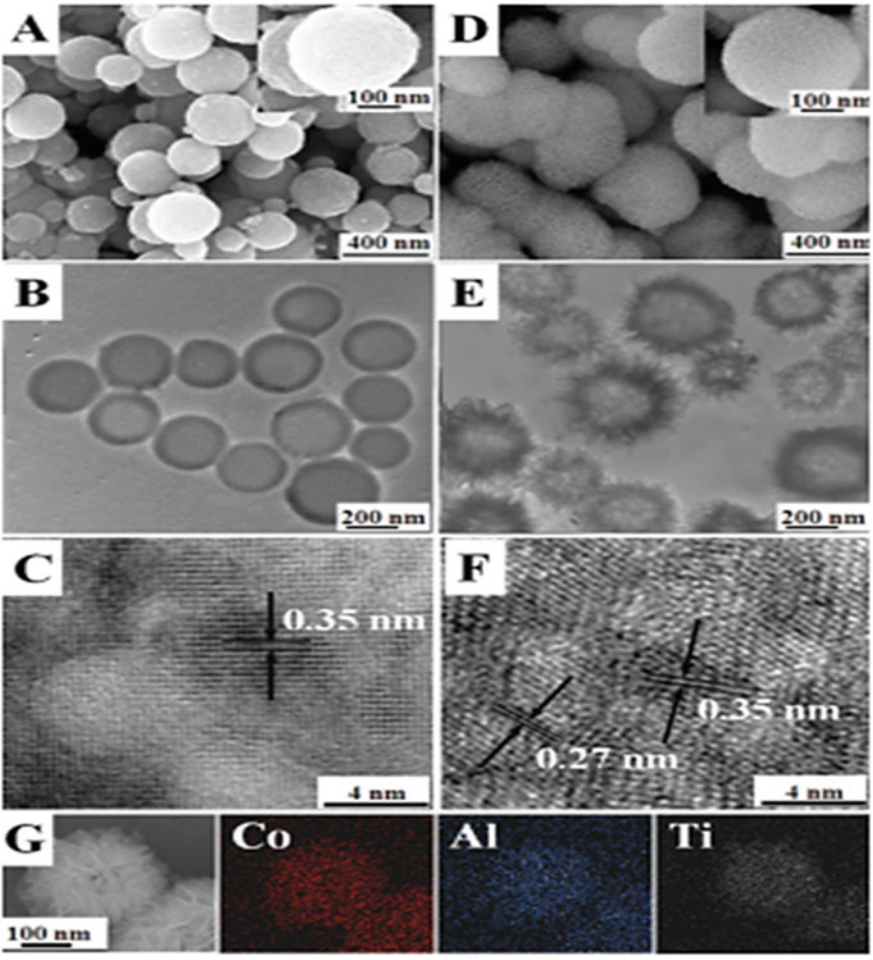

Fig. 11 **a** SEM, **b** TEM, and **c** HRTEM image of TiO_2 hollow nanospheres, **d** SEM, **e** TEM, and **f** HRTEM image of TiO_2@LDH core–shell nanospheres. g) SEM image and EDX mapping for an individual TiO2@LDH core–shell nanosphere [21]

excited by UV light due to its wide band gap of 3.0–3.2 eV, which only covers 5% of the solar spectrum. To enable visible light harvesting and prevent photogenerated electron–hole pairs from recombination, proper modification is required [22].

2.2 $BiVO_4$-Based Photocatalysts

Bi-based oxides photocatalysis ($Bi_4V_2O_{11}$, Bi_2O_3-TiO_2, Bi_2WO_6, Bi_2O_3, Bi_2WO_6/Bi/Bi_2O_3, Bi_2O_3/Bi_2WO_6 [23]) is non-toxic, chemical corrosion resistant,

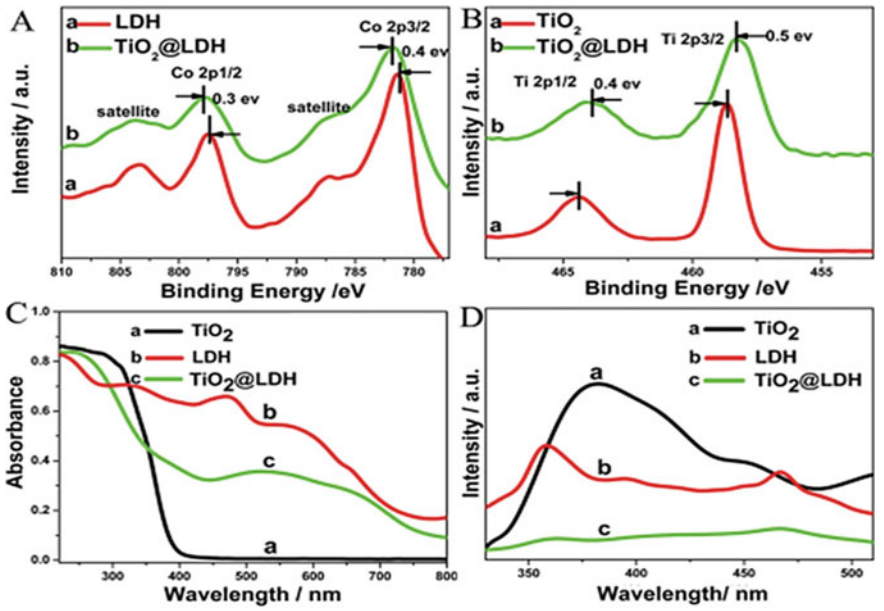

Fig. 12 **A** Co 2p and **B** Ti 2p orbital XPS spectra: **a** LDH nanoplatelets and **b** TiO_2@LDH nanospheres. **C** UV–vis DRS and **D** photoluminescence spectra: **a** TiO_2 nanospheres; **b** LDH nanoplatelets; and **c** TiO_2@LDH [21]

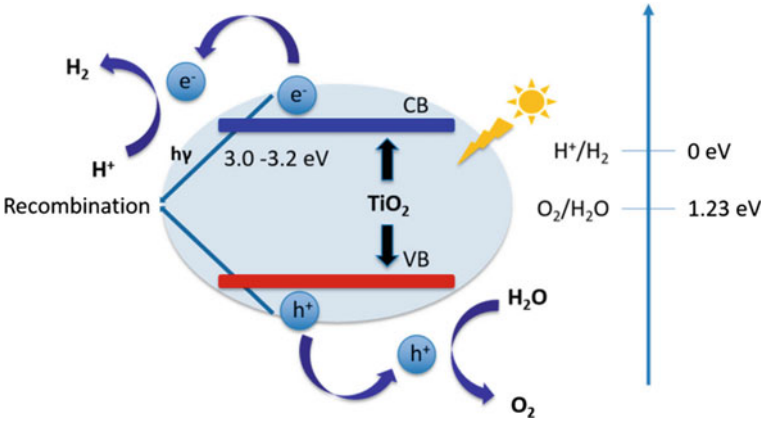

Fig. 13 Bandgap of TiO_2 taken from references (Copyright Elsevier License Number 5312530861756)

and visible light harnessing and is one of the most essential characteristics of bismuth vanadate, which makes it an effective photocatalyst. Because the energy from light absorption is used to trigger green photocatalytic processes, the latter is critical for prospective uses in renewable technology. Despite the fact that further research is needed to assess the benefits of $BiVO_4$, bismuth vanadate and its derivative materials are promising for environmental applications [24]. Due to its moderate bandgaps of 2.3–2.5 eV, excellent VB level, good photochemical stability and low-cost, the n-type semiconductor bismuth vanadate ($BiVO_4$) has attracted a lot of attention for the past few years for photocatalytic water oxidation. Monoclinic scheelite is $BiVO_4$'s most common crystalline phase, with a crystal structure made up of deformed VO_4 tetrahedrons and BiO_8 dodecahedrons as depicted in Fig. 14a–c.

Shang et al. developed a photocatalytic water oxidation system using a hybrid artificial photosynthesis system. The light harvester $BiVO_4$ and the water oxidation catalyst is a transitional metal complex ($M(dca)_2$, M = Co, Ni, DCA: dicyanamide) and the sacrificial electron acceptor is $S_2O_8^{2-}$ [25]. During the incorporation of $M(dca)_2$ in the system, the oxygen evolution activity increases. Under visible light irradiation, photocatalytic studies for oxygen evolution in $BiVO_4/M(dca)_2$ hybrid systems were performed in a completely aqueous solution containing $Na_2S_2O_8$ as a sacrificial electron acceptor ($\lambda > 420$ nm).

According to Fig. 15a, $BiVO_4/Co(dca)_2$ and $BiVO_4/Ni(dca)_2$ exhibited a higher performance than pure $BiVO_4$, which shows the catalytic role of $M(dca)_2$ in the water oxidation steps. Compared to pure $BiVO_4$, the photocatalytic oxygen evolution rate of 252.2 μmol/(h·g) during 6 h of reaction, the $BiVO_4/Co(dca)_2$ and $BiVO_4/Ni(dca)_2$ systems exhibited higher photocatalytic performances, with oxygen evolution rates of 508.1 and 297.7 μmol/(h·g) and TONs (vs. $M(dca)_2$) of 3.46 and 2.03, respectively. The $BiVO_4/Co(dca)_2$ had a photocatalytic oxygen evolution rate of 1.7 times higher than the $BiVO_4/Ni(dca)_2$ system. According to surface photovoltage (SPV) analysis and subsequent electrochemical testing, $BiVO_4/Co(dca)_2$ has a higher surface charge transfer. The stability of $BiVO_4/Co(dca)_2$ was evaluated during the 30-h photocatalytic experiment. The oxygen evolution rate was accelerated and the photocatalyst was stable when $Co(dca)_2$ was hybridized with $BiVO_4$.

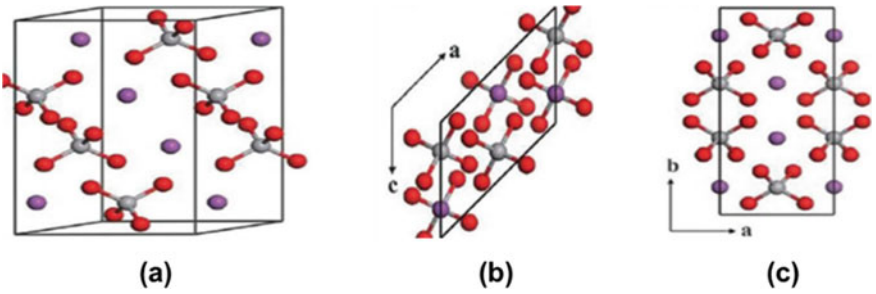

Fig. 14 **a** $BiVO_4$ crystal structure, **b** vertical view and **c** side view

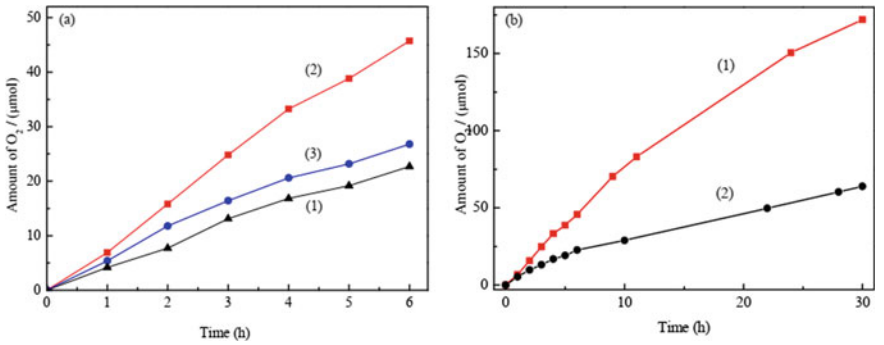

Fig. 15 **a** $BiVO_4$ Photocatalytic O_2 evolution 6 h for 1, $BiVO_4$/Co(dca)$_2$ 2, $BiVO_4$/Ni(dca)$_2$ (3) systems, **b** photocatalytic oxygen evolution for 30 h for the $BiVO_4$/Co(dca)$_2$ [25]

From Fig. 16b, $BiVO_4$/Co(dca)$_2$ had a very steady oxygen evolution rate of more than the 30 h photocatalytic reaction, yielding 171.95 mol of oxygen (TON = 13, vs. Co(dca)$_2$). $BiVO_4$/Co(dca)$_2$ had a substantially higher stability than previously reported $BiVO_4$/molecular catalyst photocatalytic systems that had activity less than 10 h. As a water oxidation catalyst, Co(dca)$_2$ is found to be more effective than Ni(dca)$_2$. The M(dca)$_2$ engineered $BiVO_4$/electrolyte interface energetics, as well as the M(dca)$_2$ catalyzed surface water oxidation, resulting in improved photocatalytic performance. The energy barrier for hole transfer to the surface of $BiVO_4$ from the bulk is reduced, thus promoting water oxidation kinetics.

The interfacial energetics in terms of interfacial band bending were investigated further using Mott-Schotky (M-S) measurements. The energy band of $BiVO_4$ bends upward at the $BiVO_4$/electrolyte contact because it is a typical n-type semiconductor. As a result, for water oxidation, there is a pushing force for hole transfer from the bulk to the surface. As indicated in Fig. 16b, the flat band potential of $BiVO_4$ was negatively shifted by 78 and 49 mV when Co(dca)$_2$ and Ni(dca)$_2$ were added, respectively.

As can be seen in Fig. 16d, a higher band bending lead to increase in the driving force for hole transfer, which promotes the water oxidation cycle. The Co(dca)$_2$ engineered $BiVO_4$/electrolyte interface exhibited a higher band bending than the Ni(dca)$_2$ engineered interface, as evidenced by the higher cathodic shift of the flat band potential in the $BiVO_4$/Co(dca)$_2$ system. This implies that the energetics of the Co(dca)$_2$ designed $BiVO_4$/electrolyte interface favored more efficient interfacial hole transfer. Electrochemical impedance spectroscopy (EIS) analysis indicates the charge of transfer behaviors at the $BiVO_4$/electrolyte interface. The semicircle diameter of the $BiVO_4$/M(dca)$_2$ Nyquist plot was smaller than that of pure $BiVO_4$ as can be seen in Fig. 16c. Smaller interfacial resistivity for charge carrier transfer with $BiVO_4$/electrolyte interface energetics engineered by M(dca)$_2$. The equivalent circuit for the results in Nyquist plots is shown in the Fig. 16c. Three sample charge transfer resistances (Rct) were in the following order: $BiVO_4$/Co(dca)$_2$ (507 Ω), $BiVO_4$/Ni(dca)$_2$ (1747 Ω), and $BiVO_4$ (5130 Ω). This revealed that the

$BiVO_4/Co(dca)_2$ system had the best OER kinetics, which was consistent with the photocatalytic performance. The inclusion of $M(dca)_2$ considerably promotes the photogenerated hole transfer from $BiVO_4$ to the electrolyte, while $Co(dca)_2$ provides interfacial charge transfer and thereafter catalyzed the OER more efficiently [25] (Fig. 17).

Wei et al. prepared $ZnO/BiVO_4$ nanoarchitectures to show the multi-electric field modulation technique for charge separation efficiency [26]. A seeded growth technique was applied for the directed development of ZnO photocatalyst on $BiVO_4$ by combining facet engineering with interfacial defect modification, resulting in a remarkable oxygen evolution rate of 68 mol h^{-1} (step i-iii in Fig. 18a). The electrical structure of 3-D nanoarchitectures was modified in the final phase (step iv in Fig. 18a) by adjusting the calcination atmospheric environment, resulting in interfacial oxygen vacancy-rich nanoarchitectures. Well-aligned nanorod arrays were successfully constructed onto the top (010) plane surfaces and isosceles tapezoidal (110) sides of $BiVO_4$ decahedrons, as evidenced by XRD and morphological studies as shown in Fig. 18b–d. From Fig. 19a, it can be observed that the O_2 evolution activities for all Ce-$BiVO_4$ samples are significantly improved compared to pristine $BiVO_4$.

The Ce-$BiVO_4$(C) sample showed the most O_2 evolution activity. The amount of O_2 evolution after 4 h of irradiation is approximately 4 times higher than that of

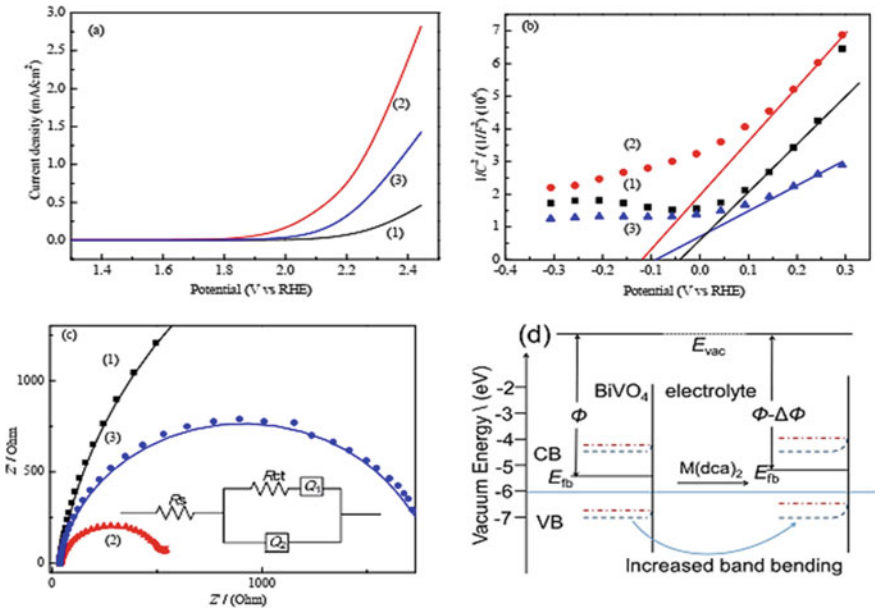

Fig. 16 $BiVO_4$ Electrochemical test results (1), $BiVO_4/Co(dca)_2$ (2), and $BiVO_4/Ni(dca)_2$ (3), **a** LSV curves; **b** Mott-Schottky plots; **c** Nyquist plots with the inset **d** structural band of the $BiVO_4$/electrolyte interface with or without the addition of $M(dca)_2$ [25]

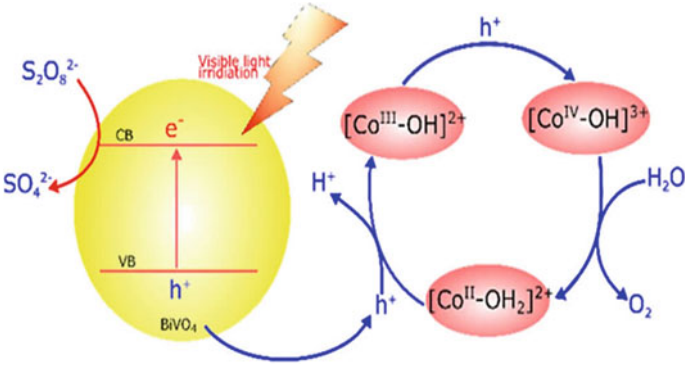

Fig. 17 $BiVO_4/Co(dca)_2$ reaction pathway of proposed photocatalytic water oxidation [25]

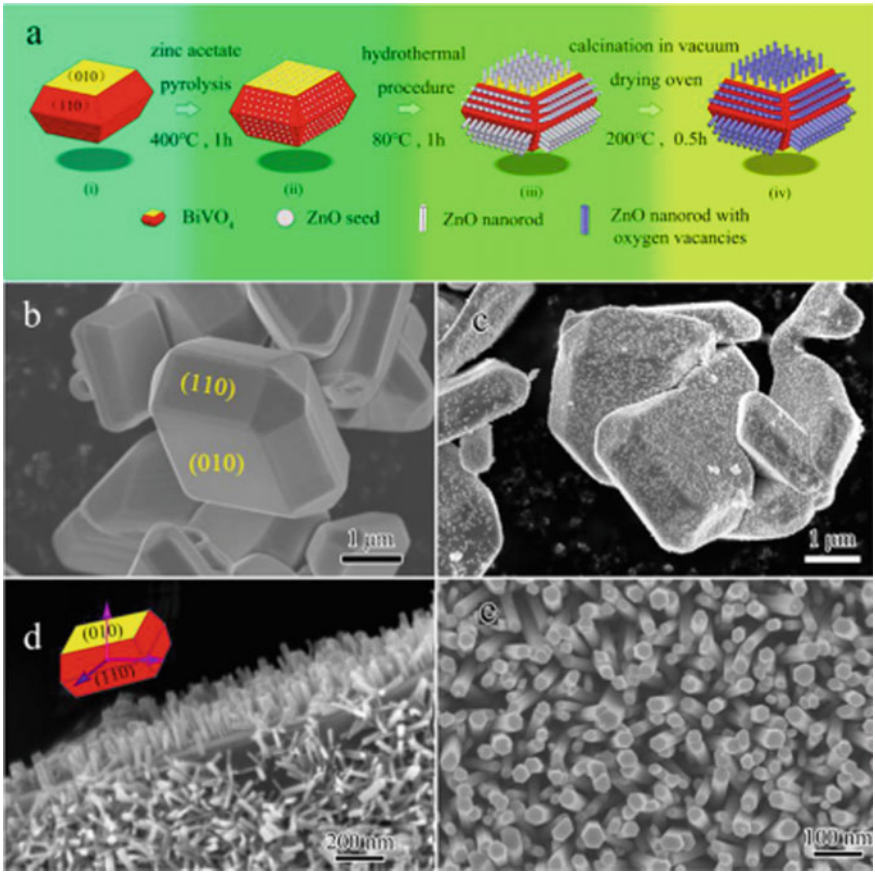

Fig. 18 **a** Preparation of $ZnO/BiVO_4$ with modulated interfacial structures and corresponding samples SEM images captured at different angle [26]

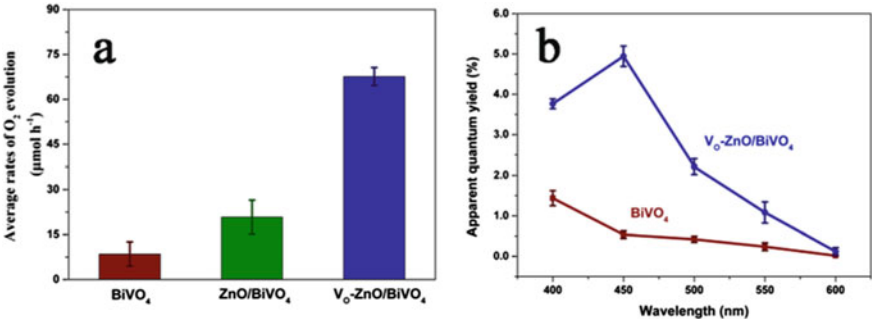

Fig. 19 **a** $BiVO_4$, $ZnO/BiVO_4$ and $Vo\text{-}ZnO/BiVO_4$ Photocatalytic water oxidation under irradiation of visible light ($\lambda > 420$ nm); **b** AQY of $BiVO_4$ and $Vo\text{-}ZnO/BiVO_4$ adopted from reference [26]

pristine $BiVO_4$. Under visible light irradiation, the photocatalytic oxygen evolution rates of $CeBiVO_4$ (C) and pristine $BiVO_4$ were evaluated (Fig. 18b). After 4 h irradiation, $CeBiVO_4$ (C) also displays a higher photocatalytic activity than $BiVO_4$ (about 4 times). According to the result, the substitution of Ce^{3+} ions in $BiVO_4$ for Bi^{3+} successfully enhances the photocatalytic activity.

The charge transfer resistance and efficiency of separation of $Ce\text{-}BiVO_4$ and pristine $BiVO_4$ were investigated using EIS. As demonstrated in Fig. 20c, $Ce\text{-}BiVO_4$ (C) has a smaller arc radius under the UV–Vis region than $BiVO_4$, implying that $Ce\text{-}BiVO_4$ (C) has a lower resistance and faster interfacial transfer of charge carrier than $BiVO_4$. The BET surface areas of pure $BiVO_4$ and $Ce\text{-}BiVO_4$ were determined to be 11.19 and 14.59 m^2g^{-1}, respectively, to better understand the major reason for photocatalytic activity (Fig. 21).

2.3 *WO_3-Based Photocatalysts*

Photocatalysts for O_2 evolution under visible light irradiation in the presence of suitable reagents are WO_3 that cause the potential at the top of the VB to be significantly higher than the potential of O_2 evolution under visible light irradiation. Another effective photocatalyst for O_2 evolution driven by visible light is $BiVO_4$. $BiVO_4$ has a band gap of 2.4 eV, which is smaller than WO_3, and also has the VB edge potential at +2.86 V versus RHE, which is sufficient for oxidizing water to create O_2 [27]. Dongsheng Li developed a deposition–precipitation procedure to prepare the Ag_3PO_4/WO_3 S-scheme heterojunction, and its photocatalytic activity was measured by monitoring water splitting and pollutant degradation under visible light. Consequently, pure Ag_3PO_4 and Ag_3PO_4/WO_3 heterojuction photocatalysts with an optimum ratio photocatalyst demonstrate an improved oxygen production photocatalytic activity at 306.6 $\mu molL^{-1}\ h^{-1}$ and 204.4 $\mu molL^{-1}\ h^{-1}$,

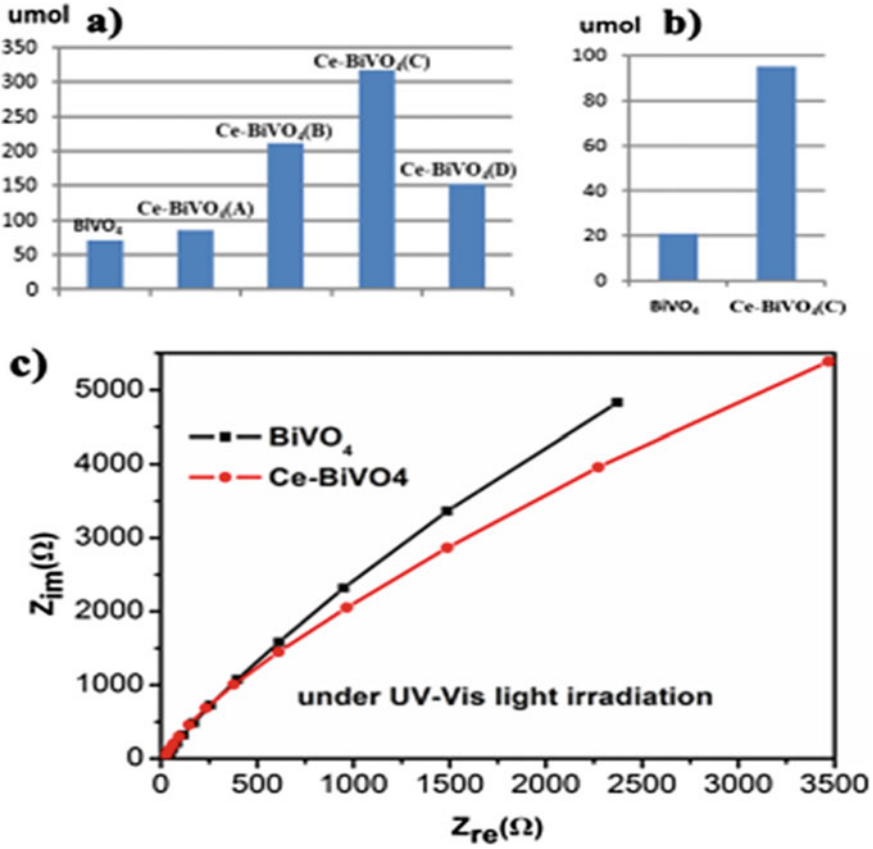

Fig. 20 **a** Photocatalytic O_2 evolution of $BiVO_4$ and Ce-$BiVO_4$ under irradiation of UV—vis light and **b** $BiVO_4$ photocatalytic O_2 evolution and Ce-$BiVO_4$ (C) in the irradiation of visible light. **c** EIS of $CeBiVO_4$ (C)/ITO and $BiVO_4$/ITO

respectively. Figure 22 demonstrate a putative S-scheme photocatalytic mechanism of Ag_3PO_4/WO_3 as indicated in detail according to a series of characterization, which supplied the heterojunction with high redox abilities to offer a tremendous photocatalytic process.

The Ag_3PO_4 has a well-defined spherical structure, smooth surface and diameter of 300 nm as shown in Fig. 23a. In contrast, the WO_3 structure was in a laminar form (Fig. 23b), whereas Ag_3PO_4 particles are tightly enveloped by WO_3 nanoparticles in Ag_3PO_4/WO_3 composites (Fig. 23c). TEM analysis of Ag_3PO_4/WO_3 composites (Fig. Schemed, e) revealed that the lattice plane spacing of 0.371 and 0.269 nm is indexed to (100) and (210) for WO_3 and Ag_3PO_4, respectively. Furthermore, interfaces between Ag_3PO_4 and WO_3 were clearly visible in the HRTEM image, demonstrating that WO_3 nanoparticles were firmly fixed on the surface of Ag_3PO_4. The EDS elemental mapping displayed that the composites are composed of Ag, P,

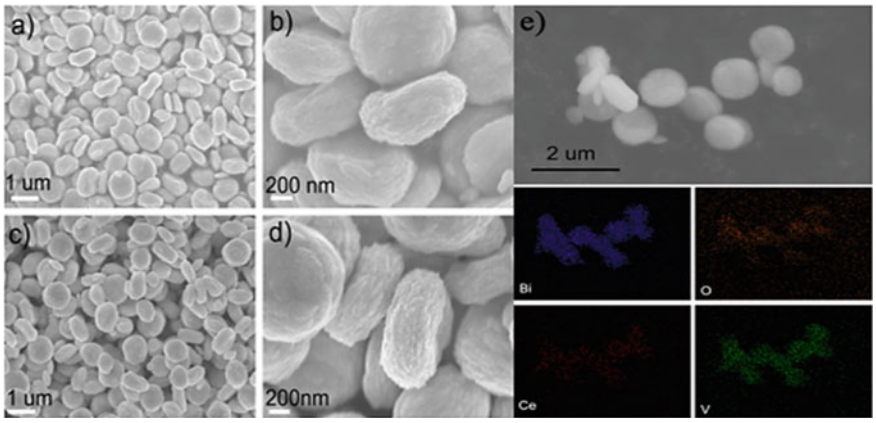

Fig. 21 Images of SEM **a**, **b**, pristine $BiVO_4$, **c**, **d** Ce-$BiVO_4$ (C), **e** Ce-$BiVO_4$ and its respective element mapping analysis

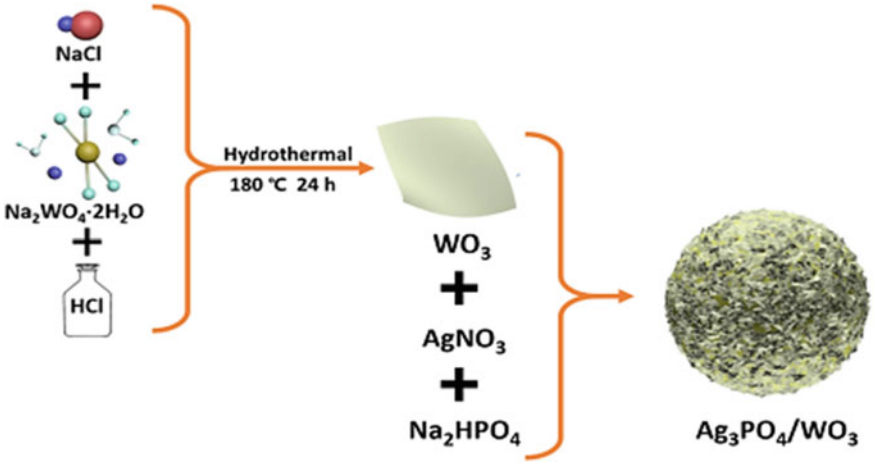

Fig. 22 Synthesis route of Ag_3PO_4/WO_3 heterojunction (Copyright Elsevier License Number 5319270917223)

W, and O elements with uniform elemental distributions (Fig. 23f), which further confirm that the WO_3 nanoparticles are distributed equally.

Figure 24a displayed the XRD profiles of the Ag_3PO_4/WO_3 heterojunction. The diffraction peaks of Ag_3PO_4 and WO_3 clearly match those of cubic Ag_3PO_4 (JCPDS card no.06–0505) and hexagonal WO_3 (JCPDS card no.33–1387), respectively. All Ag_3PO_4/WO_3 samples showed the presence of Ag_3PO_4 diffraction peaks after incorporation of WO_3, thus confirming that the phase structure of Ag_3PO_4 is not influenced by WO_3 loading. When the amount of WO_3 in Ag_3PO_4/WO_3 composites is less than

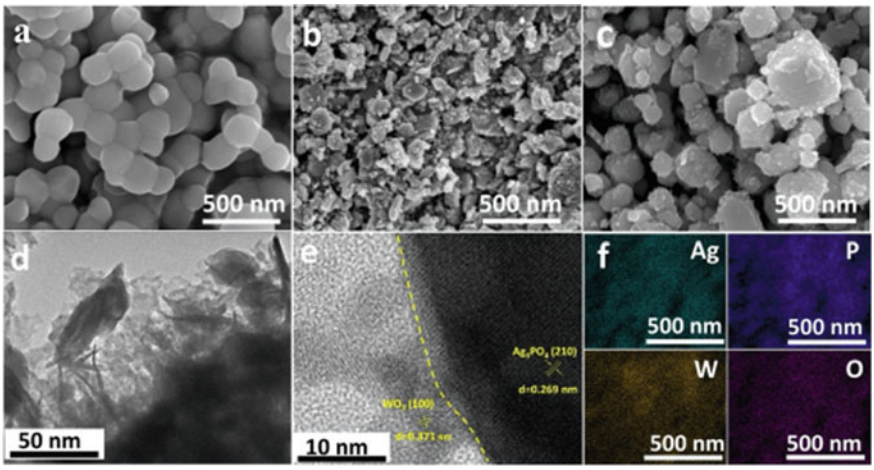

Fig. 23 **a–c** SEM images of pristine Ag_3PO_4, WO_3 and Ag_3PO_4/WO_3; TEM and HRTEM images of Ag_3PO_4/WO_3 (**d**, **e**); the elemental mapping images of Ag_3PO_4/WO_3 (Copyright Elsevier License Number 5319270917223)

5%, negligible diffraction peaks of WO_3 were observed, which can be ascribed to low loading and crystallization degree of WO_3.When WO_3 loading is higher than 5%, the diffraction characteristic peaks of WO_3 appear close to 22.89° and 28.38°, and gradually become stronger with the increase in WO_3 loading.

XPS analysis in the Ag_3PO_4/WO_3 heterojuction clearly indicates the presence of Ag, P, O, and W elements that can be seen in Fig. 24b. A doublet signal of binding energy centered at 373.6 and 367.7 eV correspond to Ag 3d5/2 and Ag 3d3/2, respectively. Figure 25b showed that the lattice oxygen atoms are represented

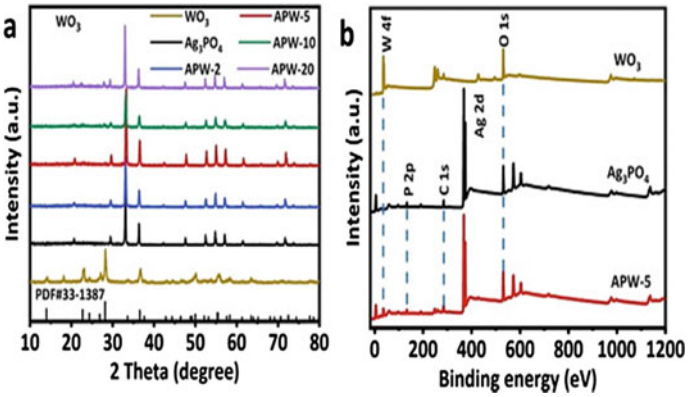

Fig. 24 **a** XRD patterns of pristine Ag_3PO_4, WO_3, Ag_3PO_4/WO_3 heterojunction, **b** XPS spectra of Ag_3PO_4/WO_3 (Copyright Elsevier License Number 5319271133782)